Supplemental Information for:

Anthropogenic control over wintertime oxidation of atmospheric pollutants

J.D. Haskins,[1] F.D. Lopez-Hilfiker,[1†] B. H. Lee,[1] V. Shah,[1††] G. M. Wolfe,[2,3] J. DiGangi,[4] D. Fibiger,[5,13 †††] E.E. McDuffie,[5,6,13 ‡] P. Veres,[5] J.C. Schroder,[5,6] P. Campuzano-Jost,[5,6] D.A. Day,[5,6] J.L. Jimenez,[5,6] A. Weinheimer,[7] T. Sparks,[8] R. C. Cohen,[8] T. Campos,[7] A. Sullivan,[9] H. Guo,[10] R. Weber,[10] J. Dibb,[11] J. Green,[12] M. Fiddler,[12] S. Bililign,[12] L. Jaeglé,[1] S.S. Brown,[6, 13] J.A. Thornton[1*]

[1] Department of Atmospheric Sciences, University of Washington, Seattle, WA USA
[2] Joint Center for Earth Systems Technology, University of Maryland Baltimore County, Baltimore, MD USA
[3]Atmospheric Chemistry and Dynamics Laboratory, NASA Goddard Space Flight Center, Greenbelt, MD USA
[4] NASA Langley Research Center, Hampton, VA USA
[5] Cooperative Institute for Research in Environmental Sciences, University of Colorado, Boulder, CO, USA
[6] Department of Chemistry, University of Colorado, Boulder, CO USA
[7] Earth Observing Laboratory, National Center for Atmospheric Research, Boulder, CO USA
[8] Department of Chemistry, University of California, Berkeley CA USA
[9] Department of Atmospheric Sciences, Colorado State University, Fort Collins, CO USA
[10] School of Earth and Atmospheric Sciences, Georgia Institute of Technology, Atlanta, GA USA
[11] Department of Earth Sciences, University of New Hampshire, Durham, NH USA
[12] Department of Physics, North Carolina A&T State University, Greensboro, NC USA
[13] Chemical Sciences Division, NOAA Earth System Research Laboratory, Boulder, CO USA

† Now at Tofwerk AG, Switzerland
†† Now at Harvard John A. Paulson School of Engineering and Applied Sciences, Harvard University, Cambridge, USA
††† Now at California Air Resources Board, Sacramento, USA
‡ Now at the Department of Physics and Atmospheric Science, Dalhousie University, Halifax, NS, Canada

* Correspondence to: thornton@atmos.washington.edu

Contents of this file:

8. References
Table S1
Figures S1-S9

1. WINTER Field Campaign Overview

The Wintertime Investigation of Transport Emissions and Reactivity (WINTER) campaign took place from February 1 – March 15, 2015. The main observing platform was the instrumented NSF/NCAR C-130 research aircraft, which was based out of the NASA Langley Research Center, located in Hampton, VA. The C-130 made a total of 13 research flights (Figure S1), typically lasting 8 hours, for a total of 96 flight hours. About 50% of flight time occurred during daylight hours while the other half occurred in the dark. Additionally, a similar number of research flight hours were spent over land as in the marine boundary layer off the eastern coast of the U.S., from north of Cape Cod, Massachusetts to central Florida. The majority (70%) of sampling occurred within the first 1.5 km of the Earth surface to focus on the near-field evolution of atmospheric pollutant in the planetary boundary layer, although all research flights included periodic vertical profiling through the boundary layer and into the middle free troposphere to characterize the composition of overlying air masses. The typical maximum altitude sampled during WINTER flights was ~ 5 km above sea level.

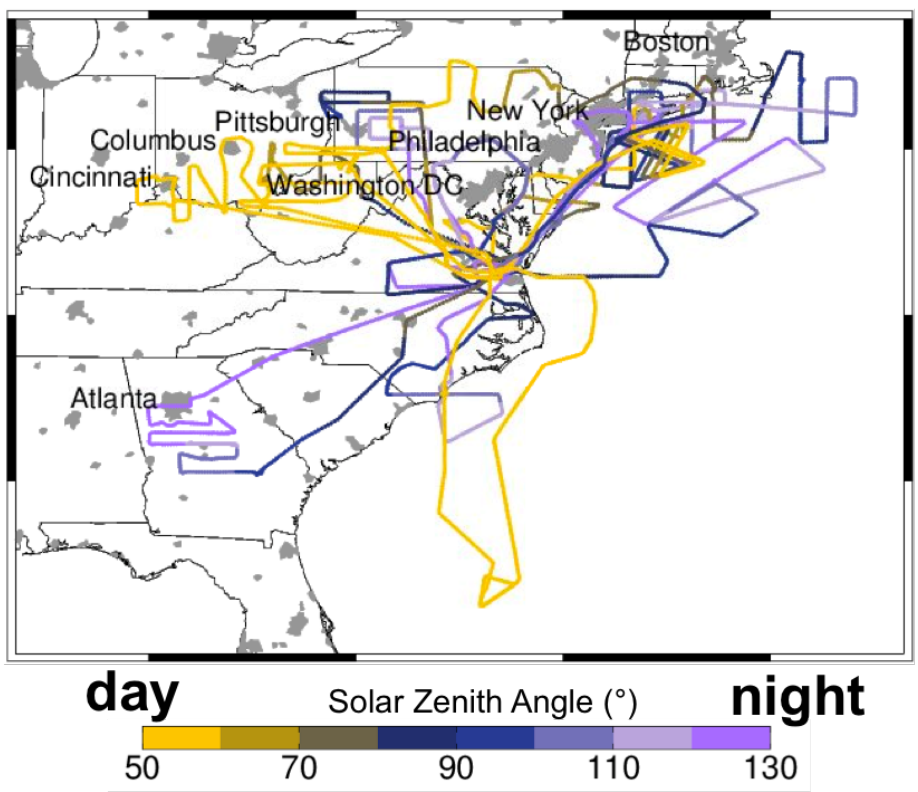

Figure S1: *Flight tracks of the 13 research flights performed during the WINTER campaign, colored by solar zenith angle with population centers highlighted in grey.*

2. Measurement methods

Table S1 lists the instrumentation operated aboard the C-130 during WINTER. Most of these instruments are well described in the literature as operated during WINTER, and the associated

references should therefore be consulted for more details. In this manuscript, we utilize observations from a iodide high-resolution time of flight chemical ionization mass spectrometer (I-ToF-CIMS), a high-resolution aerosol mass spectrometer (AMS), a cavity ringdown instrument to measure N_2O_5 via thermal dissociation and direct absorption of NO_3, a multi-channel speciated reactive nitrogen (NO_{yi}) instruments based on thermal dissociation and optical detection of NO_2, a total reactive nitrogen (NO_y) and nitric oxide (NO) instrument based on chemiluminescence from the reaction of NO with ozone (O_3), and a formaldehyde laser-induced fluorescence instrument. Sparks *et al.* (2019) provide a detailed comparison reactive nitrogen measurements on the C-130.

Supplemental Table 1: Summary of WINTER Observations Used

Measured Species	Method/ Instrument	Detection limit (10s averaging period, 2σ)	Accuracy	Measurement Frequency	Reference
J-Values	HARP-AF[a]	--	***<25-40%***	10s	Shetter & Muller (1999)
		Gas Phase	***Measurements***		
NO_2	CRDS [b,c]	45-90 pptv (at 1s)	3%	1s	Fuchs et al., (2009)
	TD-LIF [d]	90 pptv	10%	1s	Day et al., (2002)
O_3	CRDS [b]	545-650 pptv (at 1s)	4%	1s	Washenfelder et al., (2011)
	CL[e]	50 pptv	10%	1s	Weinheimer et al., (1994)
NOy	CRDS	< 90 pptv	12%	1s	Wild et al., (2014)
	CL	< 90 pptv	50%	1s	Weinheimer et al., (1994)
N_2O_5	I-TOF-CIMS [f]	0.1 pptv	30%	1s	Lee et al., (2014), Lee et al., (2018)
HNO_3	I-TOF-CIMS	2.2 pptv	30%	1s	Lee et al., (2014), Lee et al., (2018)
$ClNO_2$	I-TOF-CIMS	0.1 pptv	30%	1s	Lee et al., (2014), Lee et al., (2018)
Cl_2	I-TOF-CIMS	0.1 pptv	30%	1s	Lee et al., (2014), Lee et al., (2018)
HOCl	I-TOF-CIMS	1 pptv	30%	1s	Lee et al., (2018)
HCl	I-TOF-CIMS	22 pptv	30%	1s	Lee et al., (2014), Lee et al., (2018)
HONO	I-TOF-CIMS	40 pptv	50%	1s	Lee et al., (2014), Lee et al., (2018)
HCHO	ISAF[g]	36 pptv	10%	1s	Cazorla etal., (2015)
Speciated VOCs	TOGA[h]	--	<50%	35s, 2min	Apel et al., (2015)
		Particle	***Measurements***		
Nitrate (D_p < 4.1µm)	UNH filter [i]	--	50% passing efficiency	5 min	Dibb et al., (1999), Dibb et al., (2000), McNaughton et al., 2007
Nitrate	AMS[j]	22 ng sm^{-3} [k]	35%	1s	DeCarlo et al., (2006) Schroder et al., (2018)

a HIAPER airborne radiation package-Actinic Flux. For uncertainty description, see McDuffie et al., (2018) SI, section S1.
b Excludes research flights 01–04 due to a known problem in the sampling inlet line. Detection limits are for flights used in this analysis.
c National Oceanic and Atmospheric Administration (NOAA), Cavity Ring Down Spectrometer
d University of California Berkeley, Thermal Dissociation-Laser Induced Fluorescence detector
e National Center for Atmospheric Research Chemiliumniscence instrument for NO, NO_y, O_3
f University of Washington, high-resolution, Time-of-Flight, Iodide Chemical Ionization Mass Spectrometer
g In Situ Airborne Fomaldehyde
h NCAR, Trace Organic Gas Analyzer
i University of New Hampshire filter measurements for D_p < 4.1µm
j University of Colorado Boulder, High-Resolution Time-of -Flight Aerosol Mass Spectrometer for D_p < 1µm
k sm^{-3} refers to cubic meters at standard temperature (273.15K) and pressure (1atm) (STP)

a. University of Washington HRToF-CIMS

The UW HRToF-CIMS used Iodide adduct ionization as described previously, [Lee et al., 2014; Lee et al., 2018] to detect a suite of reactive nitrogen, halogen and organic compounds, with the most relevant for this work being N_2O_5, $ClNO_2$, Cl_2, and HNO_3, at parts per trillion detection limits. The ability of Iodide CIMS to detect these species at high time resolution (1 Hz), has been well established [Kercher et al., 2009; Mielke et al., 2011; Lee et al., 2014; Bannan et al., 2015; Iyer et al., 2016]. The general performance of the instrument and detailed upgrades to the sampling inlet,

background determinations, calibrations and ionization region during the WINTER campaign are presented in Lee et al., (2018). A few of these upgrades are discussed below in the context of the in-flight operation.

b. Formaldehyde LIF

The In Situ Airborne Formaldehyde instrument (ISAF) was used to detect gas-phase formaldehyde (HCHO) during the WINTER campaign, operating at 1 Hz, as previously described in Cazorla et al. (2015). Estimated accuracy of reported HCHO mixing ratios is estimated at ±10 %, based on calibration against IR and UV absorption of a primary HCHO standard. At 1 Hz, precision is > 20% above 100 pptv, which was typical of the nocturnal WINTER measurements used in this work (see Fig S2). At low mixing ratios, uncertainty in the signal background contributes more to the variability in precision. Detection limits at 1 Hz for a signal to noise ratio of 2 is 36 pptv for 10 mW of laser power.

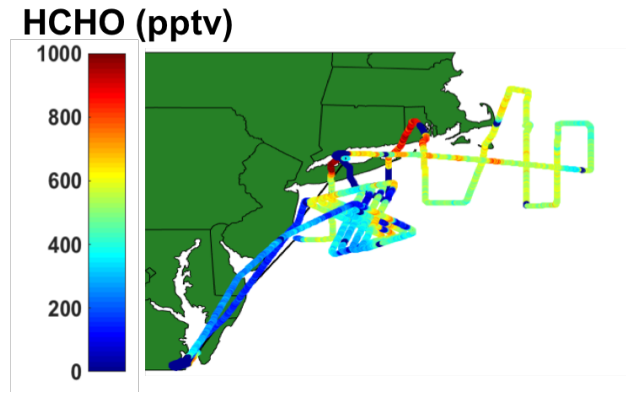

***Figure S2**: Measurements of HCHO from the nighttime Research Flights 03, and 08 made below 2000 m*

c. Chemiluminescence NO_y

NO, NO_y, and O_3 were measured with the National Center for Atmospheric Research (NCAR) Chemiluminescence Detector (CL) [Walega et al., 1991; Weinheimer et al., 1993] with accuracies for O_3, NO, and NOy of 5%, 10%, and 50% respectively [Sparks et al., 2019]. NO_y. NO_y and O_3 are sampled through a Teflon temperature controlled, rear facing inlet to avoid the intake of large particles. NO_y is measured via catalytic conversion of its component species to NO which in turn is detected by means of its chemiluminescent reaction with reagent O_3 that is added to the airstream [Walega et al., 1991]. O_3 is measured via the same chemiluminescent reaction, but produced by the addition of reagent NO to the airstream [Ridley et al., 1992].

d. Cavity Ring-Down Spectrometer

NO, NO_2, O_3, NO_y, and N_2O_5 were measured with a NOAA custom built cavity ring-down spectrometer (CRDS) following the methods described in Fuchs et al. [2009]), Washenfelder et al. [2011].), and Wild et al., (2014). The accuracy for NO_2, NO, and O_3 during WINTER were better than 4% for research flights 4-13 (McDuffie et al., 2018a). A quartz oven (650° C) was used to convert reactive nitrogen oxides (NO_y) to NO_2 (or NO) allowing for detection using methods following Wild et al. [2014]. The accuracy and detection limits for NO_y were better than 12% and between 50-380 pptv (2σ, 1s), respectively. N_2O_5 was measured after thermal dissociation (130°C) to NO_3 and subsequent subtraction of ambient NO_3, which was measured in a separate channel by direct absorption at 662 nm [Dubé et al., 2006]. The accuracy and detection limits for CRDS N_2O_5 were better than 12% and ranged from 1.3-4.4 pptv (2σ, 1s), respectively.

e. High-Resolution Aerosol Mass Spectrometer

A highly-customized high-resolution time of flight aerosol mass spectrometer (HR-ToF-AMS, Aerodyne Research Inc, referred to as "AMS") measured non-refractory composition of PM_1. The theory and operation of the AMS has previously been described in detail [Jayne et al., 2000; DeCarlo et al., 2006; Canagaratna et al., 2007; Dunlea et al., 2009; Jimenez et al., 2009; Kimmel et al., 2011]. In-field calibrations for both nitrate and chloride were performed multiple times throughout the campaign. Detection limits for nitrate and chloride were 0.07 μg sm^{-3} for a 1-sec sampling interval (sm^{-3} refers to standard cubic meters at 273 K and 1 atm). Accuracy for AMS detection of inorganic species is estimated as +/-35% [Bahreini et al., 2008]. Semi-refractory species, such as $NaNO_3$ (sodium nitrate) and Na_2SO_4 (sodium sulfate), are inefficiently detected by the AMS [Hayes et al., 2013] and AMS data have sometimes been used to estimate the fractions of ammonium nitrate and organic nitrates using the measured NO_2^+/NO^+ ion ratio from the AMS [Fry et al., 2013; Farmer et al., 2010]. However, in this study, the presence of particulate nitrite and the likely partial detection of $NaNO_3$ made that method indeterminate. For that reason, in addition to total measured nitrate, estimates were made of total inorganic nitrate concentrations based on comparisons of the AMS data to the IC-based instruments. For this campaign, the chloride signal was corrected for a recently discovered small vaporizer interference [Hu et al., 2017] when sampling under high particulate nitrate conditions. Other operational specifics for the AMS during the WINTER campaign can be found in Schroder et al., (2018).

f. TDLIF (sum PNs)

NO_2, the sum of peroxy nitrates (ΣPNs), the sum of alkyl nitrates (ΣANs), and HNO_3 were measured by the University of California Berkeley Thermal Dissociation – Laser Induced Fluorescence Instrument (TD-LIF) (Day et al., 2002; Wooldridge et al., 2010; Kenagy et al., 2018). The accuracy and detection limits of the TD-LIF measurements of ΣPNs, ΣANs, and HNO_3 depend on the accuracy of the primary measurement of NO_2, the precision of the calibration in the different detection cells, the conversion efficiency in the inlet, and the transmission efficiency of the inlet. The estimated accuracy of the NO_2 measurements during WINTER was 5%, with a detection limit of 20 pptv.

3. Observationally Constrained Radical Source Calculations

As noted in the main manuscript, we use two approaches to estimating the source of radicals important to atmospheric oxidation from the *in situ* observations made during WINTER. Both the instantaneous production rate calculation and the predicted daily integrated radical source care described below.

a. Instantaneous production rate

With the exception of alkene ozonolysis (discussed in section 5) and HO_x production from Cl reaction with alkenes, most atmospheric radicals are produced from photolysis of closed shell precursors. Therefore, the instantaneous source of radicals throughout the majority of the WINTER domain will be the sum of local photolysis rates for each precursor discussed in the main manuscript, as shown in equations S1 and S2.

$$P_i(t) = n_i j_i(t)[X_i(t)] \qquad [\text{molec./cm}^3/\text{s}] \qquad \text{(S1)}$$

$$P_{total}(t) = \sum_i n_i j_i(t)[X_i(t)] \qquad [\text{molec./cm}^3/\text{s}] \qquad \text{(S2)}$$

In equations S1 and S2, n are species specific stoichiometric coefficients representing the number of radicals produced per photolysis event of species X_i. The j_i are the time (and thus also space)

dependent photolysis frequencies of species X_i. We use *in situ* measurements of both j_i values and precursor concentrations and literature values of n_i to calculate the instantaneous radical production rate for a given species. We then sum across these rates for all species considered to obtain the total. These instantaneous radical source calculations carry the fewest assumptions, but can only be calculated from daytime data and cannot provide accurate estimates of radical sources which may have already undergone photolysis prior to intercepting the air mass with the C-130. Therefore, we also calculate estimates of a daily integrated version of equations S1 and S2, discussed below.

b. Daily integrated source

There is a wide distribution in the atmospheric lifetimes of potentially important radical sources. For example, the local noon lifetime of $ClNO_2$ is approximately 30 minutes, while that for O_3 undergoing R1 is on the order of a day. Moreover, $ClNO_2$ production is negligible during the daytime, such that for most of the day $[ClNO_2]$~0, even though its photolysis may have resulted in a significant source of Cl atoms in the first few hours after sunrise. Therefore, to obtain a more complete picture of the importance of various short-lived radical sources we calculate daily integrated radical production rates.

$$P_i(24h) = \int n_i j_i(t)[X_i(t)]dt \qquad \text{(S3)}$$

Noting that for $ClNO_2$, Cl_2, and HONO, which we assume are not produced during the day and which have lifetimes due to photolysis that are shorter than ~4 hours, then from mass balance considerations, equation S3 simplifies to

$$P_i = n_i[X_i]_{t0} \qquad \text{(S4)}$$

where $[X_i]_{t0}$ is the concentration of precursor X present at sunrise. We use the concentrations of species observed at night or in the very early morning as an approximation. In the main text, we discuss an extrapolation of values observed at night to a representative sunrise concentration, where the extrapolation is based on known chemistry (see Figure 2). But, in general we use only the observed values, which may then underestimate the appropriate concentration for use in equation S4 if there is continued production of the precursor from the measurement time to sunrise time. Thus, for $ClNO_2$ and HONO, our estimates of its contribution are likely conservative, in that they could be larger given the potential for continued production (or emission in the case of HONO) throughout the night.

For O_3 and HCHO a better approximation is that their concentrations are constant throughout the day. This assumption accounts for the slower photochemical losses and allows for some photochemical production during the day offsetting the loss due to photolysis. We did not observe a strong dependence of boundary layer average $[O_3]$ and [HCHO] on time of day, consistent with this approximation. In this case, equation S3 simplifies to equation S5.

$$P_i = n_i[X_i]_{t0} \int j_i(t)dt \qquad \text{(S5)}$$

The j_i values for equation S5 are obtained from the average measured photolysis frequencies within the boundary layer throughout the WINTER campaign. The daily integrated source calculations assume there is no significant recycling of radical precursors throughout the day, which may not be the case for HONO or Cl_2, and neglects dilution due to plume spreading or entrainment. As noted in the main text, this latter assumption depends strongly on the vertical distribution of precursors throughout the planetary boundary layer and the extent of vertical mixing that occurs throughout the day. As the C-130 was most often within the residual layer of the convectively

mixed boundary layer at night, or the mixed layer during the day, this assumption is reasonable. While high concentrations of precursors, such as HONO are highly localized in the first 100 m above the surface at night, the C-130 did not sample those concentrations very often (on the 0.1 to 1 Hz observation frequency used herein) and so the averages shown in the main manuscript minimize their impact on our conclusions.

4. F0AM Box Modeling

The Framework for 0-D Atmospheric Modeling (F0AM) was initialized using concentrations of N_2O_5, $ClNO_2$, HNO_3, and HONO from the CIMS, HCHO from the ISAF, and NO, NO_2, and O_3 from the CRDS, at the point of observation of when the maximum concentration of $ClNO_2$ was observed, which occurred on RF 08 at 06:36 local time on 3/1/2015 off the coast of Long Island. Additionally, the model was initialized earlier in that morning (06:16 local time) when $ClNO_2$ concentrations (400 pptv) were close to the median of observed $ClNO_2$ concentrations at night within the boundary layer during this flight to test the median impacts of Cl on the oxidant budget, in addition to the extremes, within the WINTER boundary. Measurements of VOCs from the NCAR Trace Organic Gas Analyzer (TOGA) were not available on this flight due to an instrumental problem. Therefore, observations from Research Flight 3, which sampled a similar spatial domain when the TOGA was operational, were used to correlate all observed VOCs with CO to derive a separate linear fit for each observable VOC (propane, formaldehye, iso-butene, n-butane, acetaldehyde, methylbromide, isopentane, n-pentane, methanol, ethanol, acrolein, propanal, acetone, 2-methylpentane, 3-methylpentane n-hexane, dichloromethane, methacrolein, butanal, methyl-ethyl-keytone, chloroform, ethylnitrate, benzene, n-heptane, dibromoethane, toluene o-xylene, 1-2-4-trimethylbenzene 1-2-3-trimethylbenzene, tertbutylnitrate, 2-butylnitrate, n-butyloxy). These fits were then used to estimate VOC concentrations on Research Flight 8 based on the measured CO as shown below in Figure S3. This model does not include the dynamics of mixing, or deposition, but does assume a constant dilution rate of 1 s^{-1}, and is initialized with concentrations within the well-mixed residual layer.

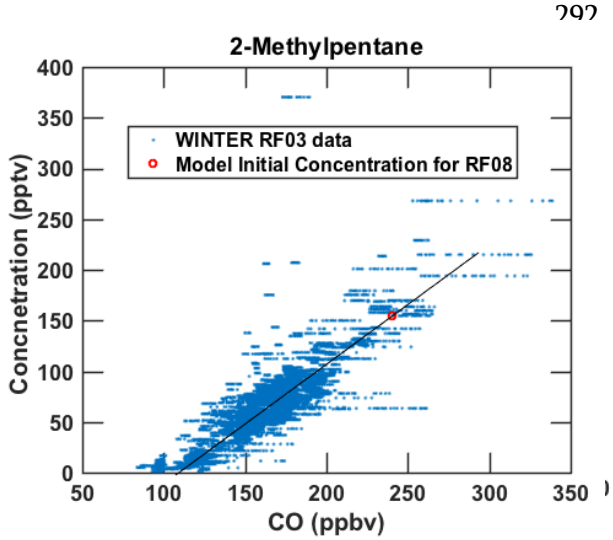

***Figure S3**: Example of method used to estimate a particular VOC's concentration from observed CO on RF08 during the TDLIF instrument malfunction from RF03 data.*

Photolysis frequencies were calculated using the TUV radiation model under the observed conditions assuming clear sky conditions and scaled to match observed photolysis frequencies at the time of intercept. The model was run for a period of 4 days to allow sufficient spin-up time, starting at the time of observation holding only CH_4 and CO constant, updating the solar parameters in 30-minute time steps. At the end of each full day, the observed concentrations were set back to their observation (at 6:36:49 local time), while concentrations of VOCs that were not initialized came into steady state and accumulated in concentration, while still undergoing a diurnal cycle. A 4 day spin up was required for these non-observed VOCs to come into steady state (same end of day and beginning of day concentrations), after which, increasing the spin up period had little effect on the non-observed VOC concentrations. The concentrations of the unobserved VOCs do not

accumulate unencumbered, as they respond to the diurnal cycle of other compounds. Fox example, in Figure S4, several observed (HCHO) and unobserved VOCs (PAN, APN) are shown. It can be seen here that the profiles of the unobserved VOCs begin the day and end the day with the same concentration at the end of the spin up period. Sensitivity simulations preformed using only a 2 day spin up period showed radical budget changes were not greater than 3%. The results presented here, therefore, are not significantly sensitive to the selected spin up time period, given that most changes occur within a single day.

At the end of the 3rd day of the spin up period, all compounds were allowed to freely evolve while CH_4 and CO were held constant. Results shown are from the 4th day of the simulation during the free evolution period. Reactions included are from the Master Chemical Mechanism version 3.3.1 and the Riedel et al. (2014) chlorine reaction mechanism. Heterogeneous N_2O_5 formation is implemented by assuming a constant source of wet aerosol surface area density of 3.61×10^{-6} cm^2

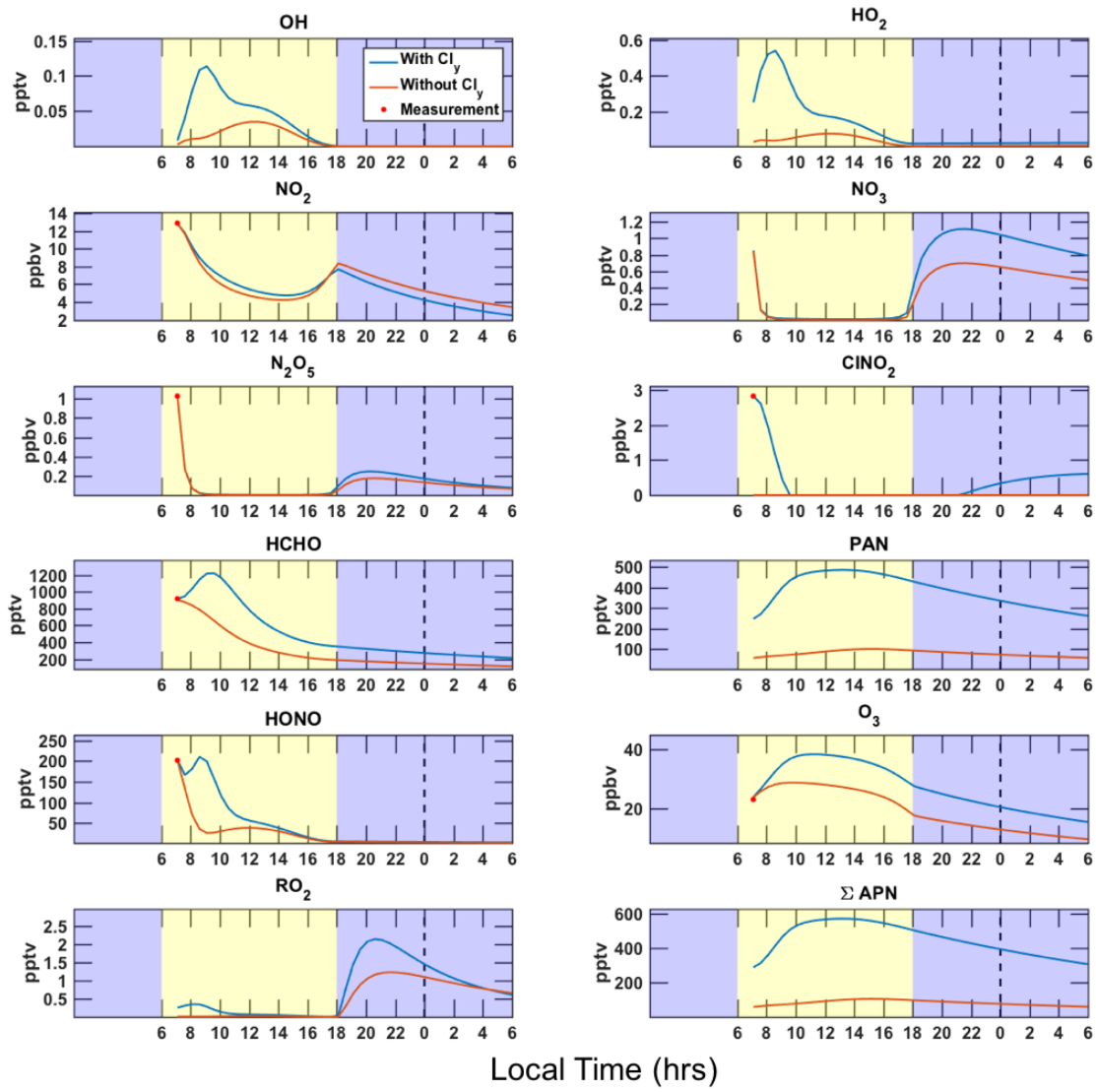

Figure S4. *Time series of F0AM modeled gas phase concentrations initialized at peak $ClNO_2$ observation at 6:36 local time considering reactions with chloride and without them during the free evolution period and measurements at the point of observation. Daytime hours are shown in yellow and nighttime hours in purple.*

cm^{-3} derived from onboard measurements of dry aerosol number distributions at the time of plume intercept, following the method described in McDuffie et al. (2018), and a constant aerosol uptake coefficient of 0.006. Heterogeneous $ClNO_2$ formation was implemented assuming a yield of 1.0. These uptake and yield values were chosen arbitrarily and do not affect the radical budget calculated following the next day since the concentrations of $ClNO_2$ and N_2O_5 are set back to observations at the end of the night before the radical budget is allowed to freely evolve as the sun rises the following morning. A time series of the modeled concentrations of relevant species is shown in Figure S4 for the simulations with and without chlorine reactions. Similar to other box models, nighttime RO_2+RO_2 reaction rates in the absence of NO are highly uncertain (Stevens et al., 1997), resulting in considerable uncertainty in the simulated nighttime RO_2 concentrations.

Excluding reactions involving chlorine in F0AM caused an underestimate in the total integrated daily radical budget by a factor of 3.75 for the simulation initialized at peak $ClNO_2$ concentrations (3.1 in the median case). Results presented in parenthesis below are all for the simulation using the initialized median $ClNO_2$ concentrations. This underestimate occurs primarily from excluding the early morning source of Cl radicals from $ClNO_2$ photolysis, but also from a 114% (40%) enhancement or 0.62 ppbv (0.1 ppbv) in the integrated daily [HCHO] that occurred because of an increase in VOC oxidation by those Cl radicals and an increase in the daily integrated ozone production of 4.7 ppbv (1.5 ppbv), thereby increasing the local source of OH from O_3 photolysis. Figure S5 a and b shows that most of the increase in the production of O_3 and HCHO that results occurs early in the day immediately following $ClNO_2$ photolysis. The increase in production of HCHO that occurs in the simulation including chlorine reactions primarily results from an increase in the concentration of CH_3O, an oxidation product of VOCs + Cl, primarily CH_4, in the early morning, but also from Cl oxidation of CH_3OH, which occurs faster than its oxidation by OH as shown in Figure S5 c and d. The loss rates of HCHO also significantly increase in the simulation

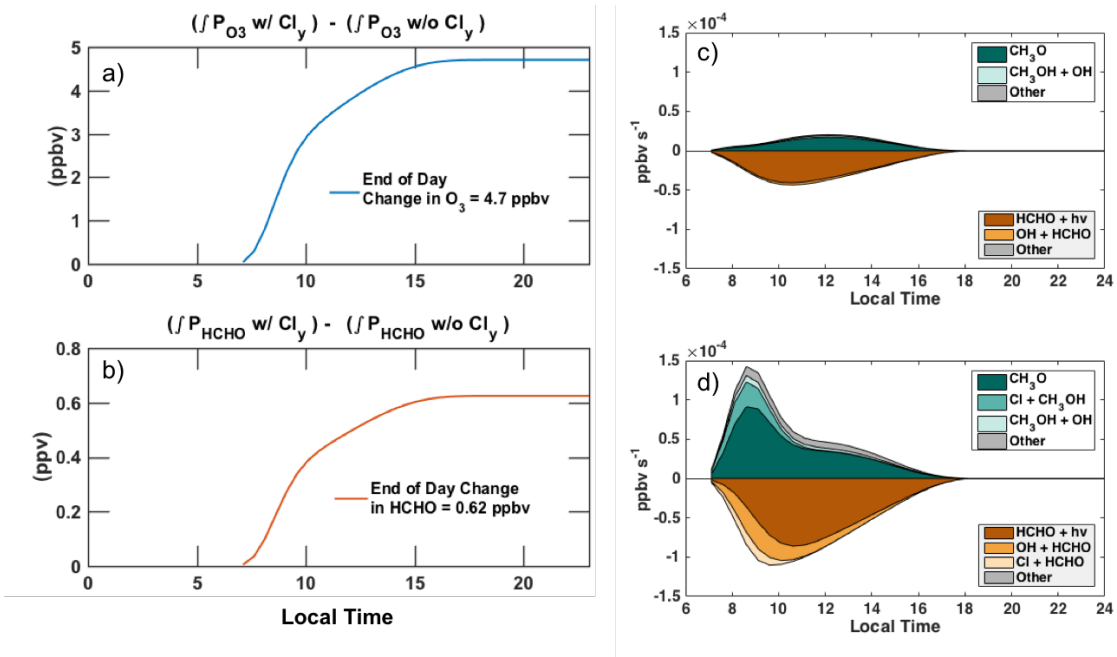

Figure S5. *a) Difference in the daily Integrated production of O_3 that results from including Cl_y reactions for the simulation initialized at the peak observed $ClNO_2$ concentration. b) Difference in the daily integrated production of HCHO that results from including Cl_y reactions. c) Top production and loss mechanisms of HCHO in the simulation not considering Cl_y reactions compared to d) the top production and loss mechanisms of HCHO in the simulation considering Cl_y reactions.*

including chlorine reactions compared to that without, though not at the same time of day as the production of HCHO does, such that the simulation including Cl_y reactions shows the largest difference in predicted HCHO concentration in the hours immediately following $ClNO_2$ photolysis at around 11am local time (Figure S4). It is possible that the enchancement in HO_x shown above, could be larger, given that the measured VOC concentrations used in the spin up are a lower limit to total VOC concentrations, since they exclude some number of alkenes that are highly reactive with Cl, such as fossil fuel derived alkenes (not including aromatics), that may not be well represented in a box model that does not take into account direct emissions. Therefore, the total speciation of alkenes in the wintertime may extend the anthropogenic impact of emissions on the oxidant budget during winter beyond what we are able to constrain and show here, zby impacting HCHO, and therefore HOx yields.

5. Radical production from alkene ozonolysis

Ozonolysis of alkenes produces hydroxyl radicals (OH) from the decomposition of the Criegee intermediate. The TOGA instrument measured a large suite of biogenic alkenes and a smaller set of fossil fuel derived alkenes (not including aromatics). Based on these observed species, alkene ozonolysis was generally negligible, being on average less than 5% of the source from ozone and formaldehyde photolysis (see Figure S6). In the Northeastern U.S. during winter, emissions of biogenic alkenes are expected to be nearly zero in the case of isoprene, or very low in the case of monoterpenes. The fossil fuel derived alkenes, isobutene and acrolein, contributed equally to radical production as the sum of seven terpenes or their oxidation products (see Figure S6). Thus, it is possible that close to fossil fuel or industry related emissions, alkene ozonolysis might be a locally important radical source, but given the short lifetime of alkenes the regional importance is likely significantly less than that of the other radical precursors considered here.

6. Estimates of HONO production from pNO_3^-

The photolysis of nitrate on surfaces and in the condensed phase to produce NO_x and HONO has been well documented in laboratory studies and snow packs [Zhou et al., 2003; Zhu et al., 2010; Du et al., 2011; Baergen et al., 2013;]. Recently, Ye et al. (2016) showed that nitrate photolysis in aerosol particles (pNO_3^-) could produce HONO at rates capable of explaining HONO mixing ratios observed in the summertime marine boundary layer of the western Atlantic Ocean, just south of the typical WINTER flight domain. Romer et al., (2018) provided an upper limit on how much more efficiently pNO_3^- could photolyze relative to HNO_3, during 6 different

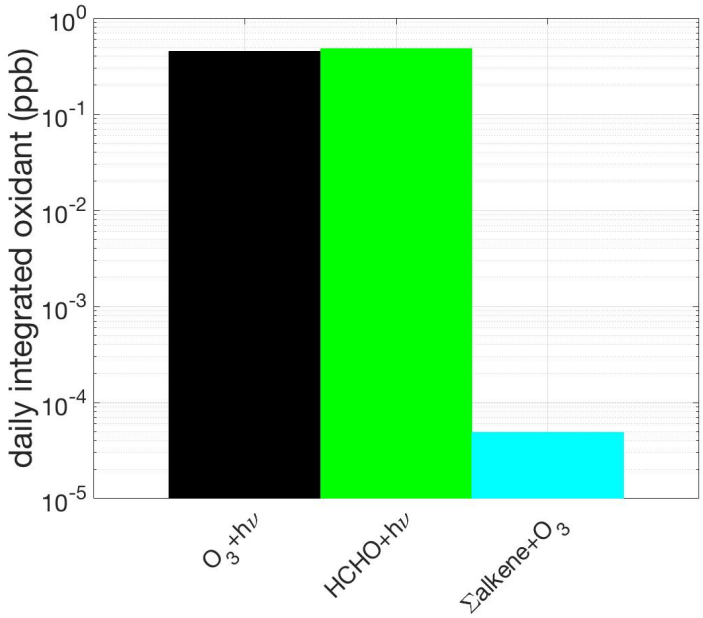

Figure S6. Comparison of the relative contributions of O_3 and HCHO photolysis and the alkene ozonoylsis reactions to the daily integrated radical budget during WINTER

aircraft campaigns, given that the fastest proposed photolysis rate are inconsistent with observed NO_x to HNO_3 ratios. Using the proposed parameterization of pNO_3^- photolysis, which is referenced to gas-phase HNO_3 photolysis frequencies, and constrained with observed values of $j(HNO_3)$ and j(HONO), we predicted daytime HONO mixing ratios using both a pNO_3^- photolysis enhancement factor (EF) of 300 (Ye et al., 2016) and 30 (Romer et al., 2018) with the AMS pNO_3^- measurements and the filter measurements of pNO_3^- that were made in WINTER.

The comparison between predicted and observed daytime enhancements in HONO observed below 1 km for the WINTER campaign are shown in Figure S7. Potential biases could arise from direct emissions of HONO sampled near urban areas and ships. Therefore, we show results where we bin the comparison to different ranges in the NO_x/NO_y, which is an indicator of air mass age since NO_x emissions occurred. In all plumes, better correlation between parameterization predictions of HONO and observations are seen using the filter measurement of pNO_3^- ($D_p < 4.1$ μm) than the AMS pNO_3^- ($D_p < 1$μm). This is likely because of the more complete sampling of the size distribution of pNO_3^- captured from the filter measurements given the low cutoff of the AMS inlet during WINTER. At the lowest NO_x/NO_y ratio, in air less affected by direct HONO emissions, the observed enhancement of HONO is low and better correlated using a pNO_3^- EF of 30, but regardless of which pNO_3^- measurement is used, the enhancement in HONO is near the limit of detection of the I^- CIMS (see above). This indicates that in aged air, if HONO is indeed created from secondary processes like the photolysis of pNO_3^-, the enhancement is too low for our instrument to confidently detect.

At the highest NO_x/NO_y ratios, in areas of fresh NO_x emissions, the observed and predicted HONO concentrations are better correlated using an EF of 300. However, direct emission of HONO from industrial processes in NO_x rich air could be contributing to the observed concentrations, in which case, this method of analysis is not appropriate for extracting an EF. Predictions from the F0AM modeling presented above indicate that requiring a sink of total nitrate using an EF of 300 under WINTER conditions would be an order of magnitude faster than $OH+NO_2$ creating total nitrate, such that the total nitrate lifetime becomes unrealistically short (e.g. < 12 hours) with predicted total nitrate concentrations falling to 0 before sunset.

The results in Figure S7 suggest that pNO_3^- photolysis as fast as the Ye et al. (2016) parameterization, would tend to overestimate HONO during the WINTER campaign away from relatively fresh NO_x emissions, while using a pNO_3^- photolysis EF of 10-30 from Romer et al., (2018), would generally tend to explain observed HONO. However, given that all of the far field measurements of HONO during WINTER are at or below the limit of detection, our measurements cannot quantify an appropriate EF for pNO_3^- photolysis producing daytime HONO, but do provide further evidence of an EF lower than 300, given the chemical lifetime inconsistencies that would arise if total nitrate was lost so quickly at the observed conditions. We conclude from this analysis that pNO_3^- photolysis may be an important source of daytime HONO but that our data does not robustly support such a source. Uncertainties in the HONO observations, which in the daytime are typically within a factor of 2 of our estimated limit of detection, and the limited availability of data having both high pNO_3^- and $jHNO_3$ preclude a more direct conclusion.

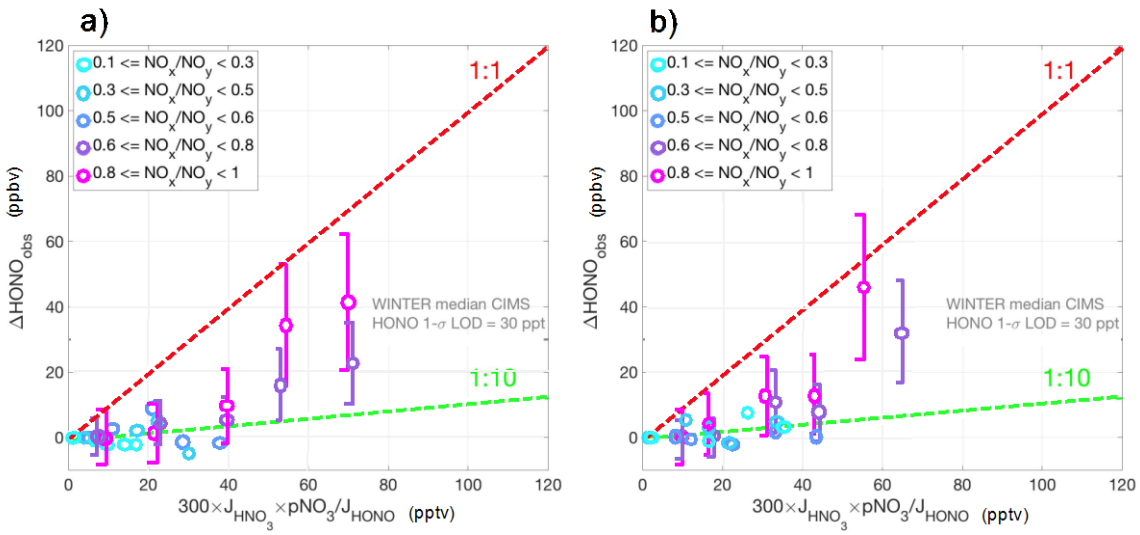

Figure S7. *The median observed enhancement in HONO concentrations relative to the lowest binned observation during the day in WINTER below 1 km, compared to the predicted values of HONO using the parameterization from Ye et al., (2016). Comparisons are binned and colored by the NOx to NOy ratio as an indicator of plume age. Predictions are calculated with observed photolysis frequencies and either (a) AMS particle nitrate concentrations or (b) filter particle nitrate concentrations, using a photolysis enhancement factor of 300 (red line) from Ye et al., (2016) or an enhancement factor of 30 (green line) from Romer et al., (2018). Error bars shown indicate the 50% uncertainty in I^- CIMS HONO measurements and are shown only for cases where observed HONO concentrations included in the analysis were greater than the HONO detection limit.*

Given that the above analysis does not rule out a role for pNO_3^- photolysis as a source of HONO, for comparison with the results shown in the main manuscript, we include in our estimates of the daily integrated radical source pNO_3^- photolysis to form HONO as prescribed by Ye et al. (2016) using a pNO_3^- photolysis EF of either 300 or 30 [Romer et al., 2018]. The results of those calculations, similar to those shown in Figure 4, are presented in Figure S8. The importance of the HONO source from pNO_3^- photolysis is largest in polluted air (light and dark gray bars). The relative importance of pNO_3^- photolysis as a daytime HONO production channel, and therefore OH source relative to other oxidant sources, largely depends the photolysis EF chosen, underscoring the need for further constraints on this process. At maximum, both over land and in the MBL pNO_3^- photolysis could account for up to 11 – 33% of the total daily radical source if using an EF of 300, though this is likely an overestimation. More in line with our far field HONO measurements, this pathway only accounts for 1-4% of the total daily radical source if using an EF of 30 (Romer et al., 2018).

7. Radical source statistics

Figure S9 shows a broader comparison of the different radical sources constrained by the WINTER observations. The panels show cumulative distribution functions for the contribution of each specific radical source to the total daily integrated source derived from measurements over land (a)

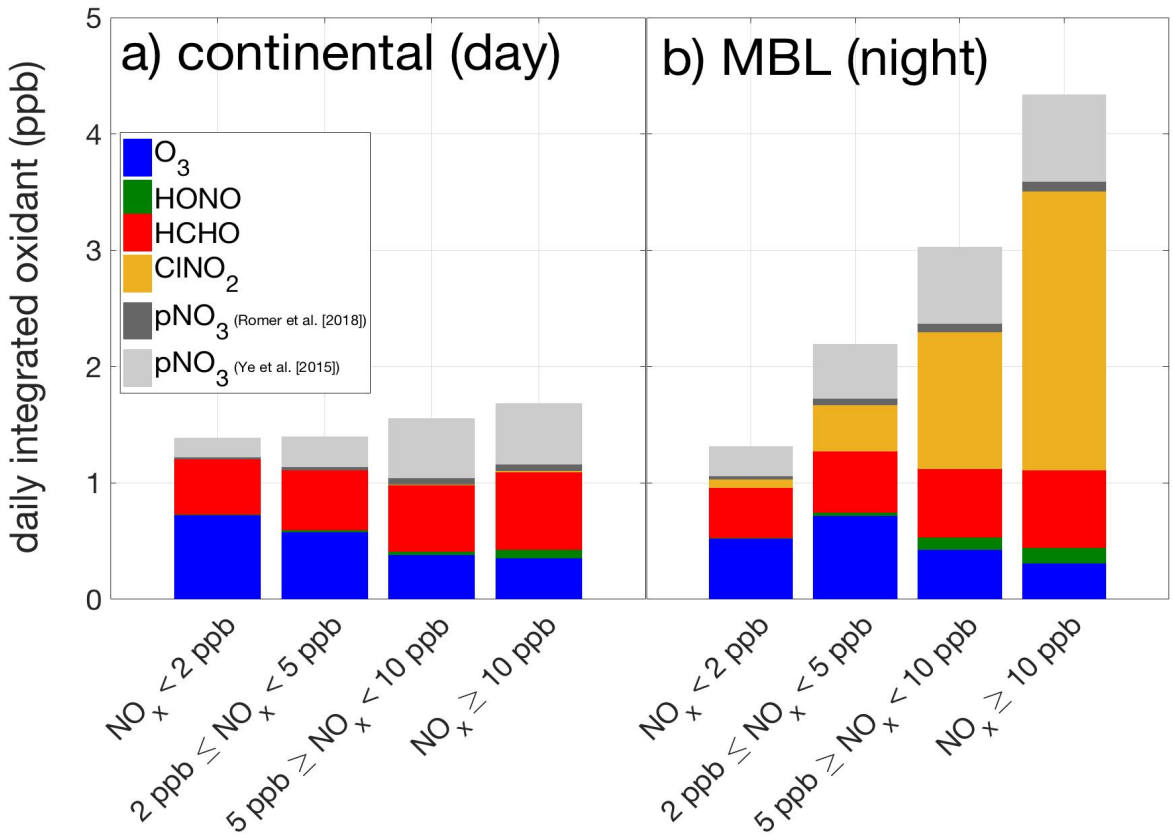

Figure S8. The predicted contribution of each radical precursor to the daily integrated oxidant budget when considering daytime production of HONO following pNO_3^- photolysis at rates prescribed by Ye et al., (2016) and Romer et al., (2018) during winter, binned by NOx concentration at the time of early morning observation during the day over continental regions and during the night in the MBL when we were sampling within the boundary layer.

and in the marine boundary layer (b) to demonstrate how often a particular radical source made a given contribution to the overall radical budget. We relaxed our selection criteria compared to the calculations shown in Figure 4 of the main manuscript, requiring only that NO_x> 2ppb and the C-130 altitude < 1 km, but otherwise the data used for Figure S9 is the same as in Figure 4. These distributions illustrate that over land, $ClNO_2$ is only rarely a major component of the daily radical source, contributing less than 20% of the total radical source in more than 80% of the determinations. In half the measurements over land, HCHO and HONO accounted for ~50% and ~30%, respectively, of the total daily radical source. In over half the measurements in the MBL, $ClNO_2$ represented about 40% of the total daily radical source, with minimal importance from HONO. These statistics do not include a potential source of HONO from pNO_3^- photolysis.

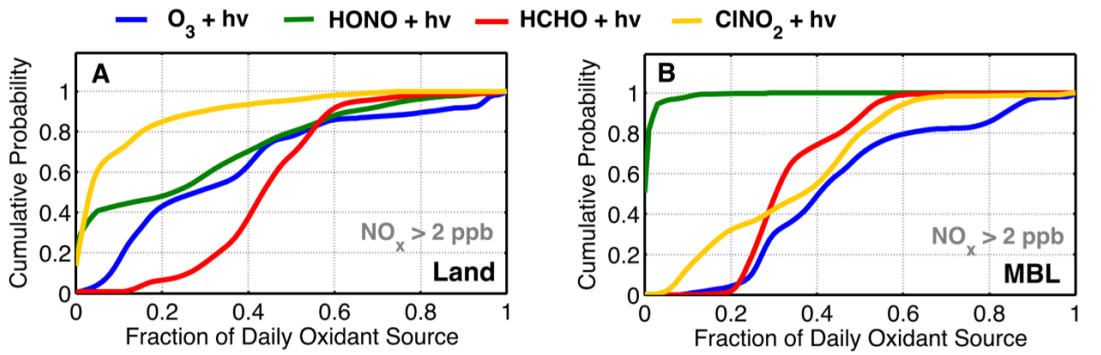

Figure S9. The cumulative distribution functions for the contribution of each specific radical source to the total daily integrated source derived from measurements (a) over land and (b) in the marine boundary layer at all points during the campaign where NO_x > 2ppbv.

8. References

Baergen, A. M., & Donaldson, D. J. (2013). Photochemical Renoxification of Nitric Acid on Real Urban Grime. *Environmental Science & Technology*, *47*(2), 815–820. https://doi.org/10.1021/es3037862

Bahreini, R., Dunlea, E. J., Matthew, B. M., Simons, C., Docherty, K. S., DeCarlo, P. F., … Middlebrook, A. M. (2008). Design and Operation of a Pressure-Controlled Inlet for Airborne Sampling with an Aerodynamic Aerosol Lens. *Aerosol Science and Technology*, *42*(6), 465–471. https://doi.org/10.1080/02786820802178514

Bannan, T. J., Booth, A. M., Bacak, A., Muller, J. B. A., Leather, K. E., Le Breton, M., … Percival, C. J. (2015). The first UK measurements of nitryl chloride using a chemical ionization mass spectrometer in central London in the summer of 2012, and an investigation of the role of Cl atom oxidation. *Journal of Geophysical Research: Atmospheres*, *120*(11), 5638–5657. https://doi.org/10.1002/2014JD022629

Bertram, T. H., & Thornton, J. A. (2009). Toward a general parameterization of N_2O_5 reactivity on aqueous particles: the competing effects of particle liquid water, nitrate and chloride. *Atmos. Chem. Phys.*, *9*(21), 8351–8363. https://doi.org/10.5194/acp-9-8351-2009

Bertram, T. H., Thornton, J. A., & Riedel, T. P. (2009). An experimental technique for the direct measurement of N_2O_5 reactivity on ambient particles. *Atmos. Meas. Tech.*, *2*(1), 231–242. https://doi.org/10.5194/amt-2-231-2009

Canagaratna, M. R., Jayne, J. T., Jimenez, J. L., Allan, J. D., Alfarra, M. R., Zhang, Q., … Worsnop, D. R. (2007). Chemical and microphysical characterization of ambient aerosols with the aerodyne aerosol mass spectrometer. *Mass Spectrometry Reviews*, *26*(2), 185–222. https://doi.org/10.1002/mas.20115

Cazorla, M., Wolfe, G. M., Bailey, S. A., Swanson, A. K., Arkinson, H. L., & Hanisco, T. F. (2015). A new airborne laser-induced fluorescence instrument for in situ detection of formaldehyde throughout the troposphere and lower stratosphere. *Atmos. Meas. Tech.*, *8*(2), 541–552. https://doi.org/10.5194/amt-8-541-2015

DeCarlo, P. F., Kimmel, J. R., Trimborn, A., Northway, M. J., Jayne, J. T., Aiken, A. C., … Jimenez, J. L. (2006). Field-Deployable, High-Resolution, Time-of-Flight Aerosol Mass Spectrometer. *Analytical Chemistry*, *78*(24), 8281–8289. https://doi.org/10.1021/ac061249n

Du, J., & Zhu, L. (2011). Quantification of the absorption cross sections of surface-adsorbed nitric acid in the 335–365nm region by Brewster angle cavity ring-down spectroscopy. *Chemical Physics Letters*, *511*(4), 213–218. https://doi.org/https://doi.org/10.1016/j.cplett.2011.06.062

Dube, W. P., Brown, S. S., Osthoff, H. D., Nunley, M. R., Ciciora, S. J., Paris, M. W., … Ravishankara, a R. (2006). Aircraft instrument for simultaneous, in situ measurement of NO3 and N2O5 via pulsed cavity ring-down spectroscopy. *Review of Scientific Instruments*, *77*(3). https://doi.org/10.1063/1.2176058

Fuchs, H., Dubé, W. P., Lerner, B. M., Wagner, N. L., Williams, E. J., & Brown, S. S. (2009). A Sensitive and Versatile Detector for Atmospheric NO2 and NOX Based on Blue Diode Laser Cavity Ring-Down Spectroscopy. *Environmental Science & Technology*, *43*(20), 7831–7836. https://doi.org/10.1021/es902067h

Fuchs, H., Dubé, W. P., Ciciora, S. J., & Brown, S. S. (2008). Determination of inlet transmission and conversion efficiencies for in situ measurements of the nocturnal nitrogen oxides, NO3, N 2O5 and NO2, via pulsed cavity ring-down spectroscopy. *Analytical Chemistry*, *80*(15), 6010–6017. https://doi.org/10.1021/ac8007253

Hayes, P. L., Ortega, A. M., Cubison, M. J., Froyd, K. D., Zhao, Y., Cliff, S. S., … Jimenez, J. L. (2013). Organic aerosol composition and sources in Pasadena, California, during the 2010 CalNex campaign. *Journal of Geophysical Research Atmospheres*, *118*(16), 9233–9257. https://doi.org/10.1002/jgrd.50530

Hu, W., Campuzano-Jost, P., Day, D. A., Croteau, P., Canagaratna, M. R., Jayne, J. T., … Jimenez, J. L. (2017). Evaluation of the new capture vaporizer for aerosol mass

spectrometers (AMS) through field studies of inorganic species. *Aerosol Science and Technology*, *51*(6), 735–754. https://doi.org/10.1080/02786826.2017.1296104

Iyer, S., Lopez-Hilfiker, F., Lee, B. H., Thornton, J. A., & Kurtén, T. (2016). Modeling the Detection of Organic and Inorganic Compounds Using Iodide-Based Chemical Ionization. *The Journal of Physical Chemistry A*, *120*(4), 576–587. https://doi.org/10.1021/acs.jpca.5b09837

Jayne, J. T., Leard, D. C., Zhang, X., Davidovits, P., Smith, K. A., Kolb, C. E., & Worsnop, D. R. (2000). Development of an Aerosol Mass Spectrometer for Size and Composition Analysis of Submicron Particles. *Aerosol Science and Technology*, *33*(1–2), 49–70. https://doi.org/10.1080/027868200410840

Jimenez, J. L., Canagaratna, M. R., Donahue, N. M., Prevot, A. S. H., Zhang, Q., Kroll, J. H., … Worsnop, D. R. (2009). Evolution of Organic Aerosols in the Atmosphere. *Science*, *326*(5959), 1525 LP-1529. https://doi.org/10.1126/science.1180353

Kenagy, H. S., Sparks, T. L., Ebben, C. J., Wooldrige, P. J., Lopez-Hilfiker, F. D., Lee, B. H., et al. (2018). NO_x lifetime and NO_y partitioning during WINTER. *Journal of Geophysical Research: Atmospheres*, 123, 9813– 9827. https://doi.org/10.1029/2018JD028736

Kercher, J. P., Riedel, T. P., & Thornton, J. A. (2009). Chlorine activation by N_2O_5: simultaneous, in situ detection of $ClNO_2$ and N_2O_5 by chemical ionization mass spectrometry. *Atmos. Meas. Tech.*, *2*(1), 193–204. https://doi.org/10.5194/amt-2-193-2009

Kercher, J. P., Riedel, T. P., & Thornton, J. A. (2009). Chlorine activation by N_2O_5: simultaneous, in situ detection of $ClNO_2$ and N_2O_5 by chemical ionization mass spectrometry. *Atmos. Meas. Tech.*, *2*(1), 193–204. https://doi.org/10.5194/amt-2-193-2009

Kimmel, J. R., Farmer, D. K., Cubison, M. J., Sueper, D., Tanner, C., Nemitz, E., … Jimenez, J. L. (2011). Real-time aerosol mass spectrometry with millisecond resolution. *International Journal of Mass Spectrometry*, *303*(1), 15–26. https://doi.org/10.1016/j.ijms.2010.12.004

Lee, B. H., Lopez-hilfiker, F. D., Mohr, C., Kurten, T., Worsnop, D. R., & J.A. Thornton (2014). Supplemental Information for: An Iodide-Adduct High-Resolution Time-of-Flight Chemical- Ionization Mass Spectrometer: Application to Atmospheric Inorganic and Organic Compounds. https://doi.org/10.1021/es500362a

Lee, B. H., Lopez-Hilfiker, F. D., Veres, P. R., McDuffie, E. E., Fibiger, D. L., Sparks, T. L., … Thornton, J. A. (2018). Flight Deployment of a High-Resolution Time-of-Flight Chemical Ionization Mass Spectrometer: Observations of Reactive Halogen

and Nitrogen Oxide Species. *Journal of Geophysical Research: Atmospheres*, *123*(14), 7670–7686. https://doi.org/10.1029/2017JD028082

Lopez-Hilfiker, F. D., Iyer, S., Mohr, C., Lee, B. H., D'ambro, E. L., Kurtén, T., & Thornton, J. A. (2016). Constraining the sensitivity of iodide adduct chemical ionization mass spectrometry to multifunctional organic molecules using the collision limit and thermodynamic stability of iodide ion adducts. *Atmospheric Measurement Techniques*, *9*(4), 1505–1512. https://doi.org/10.5194/amt-9-1505-2016

McDuffie, E. E., Fibiger, D. L., Dubé, W. P., Lopez‐Hilfiker, F., Lee, B. H., Thornton, J. A., et al. (2018). Heterogeneous N2O5 uptake during winter: Aircraft measurements during the 2015 WINTER campaign and critical evaluation of current parameterizations. Journal of Geophysical Research: Atmospheres, 123, 4345–4372. https://doi.org/10.1002/2018JD028336Fry, J. L., Draper, D. C., Zarzana, K. J., Campuzano-Jost, P., Day, D. A., Jimenez, J. L., … Grossberg, N. (2013). Observations of gas- and aerosol-phase organic nitrates at BEACHON-RoMBAS 2011. *Atmos. Chem. Phys.*, *13*(17), 8585–8605. https://doi.org/10.5194/acp-13-8585-2013

Mielke, L. H., Furgeson, A., & Osthoff, H. D. (2011). Observation of ClNO2 in a Mid-Continental Urban Environment. *Environmental Science & Technology*, *45*(20), 8889–8896. https://doi.org/10.1021/es201955u

Ridley, B. A., Grahek, F. E., & Walega, J. G. (1992). A Small High-Sensitivity, Medium-Response Ozone Detector Suitable for Measurements from Light Aircraft. *Journal of Atmospheric and Oceanic Technology*, *9*(2), 142–148. https://doi.org/10.1175/1520-0426(1992)009<0142:ASHSMR>2.0.CO;2

Riedel, T. P., Bertram, T. H., Crisp, T. A., Williams, E. J., Lerner, B. M., Vlasenko, A., … Thornton, J. A. (2012). Nitryl chloride and molecular chlorine in the coastal marine boundary layer. *Environmental Science and Technology*. https://doi.org/10.1021/es204632r

Ryder, O. S., Ault, A. P., Cahill, J. F., Guasco, T. L., Riedel, T. P., Cuadra-Rodriguez, L. A., … Bertram, T. H. (2014). On the Role of Particle Inorganic Mixing State in the Reactive Uptake of N2O5 to Ambient Aerosol Particles. *Environmental Science & Technology*, *48*(3), 1618–1627. https://doi.org/10.1021/es4042622

Stevens, P., Mather, J., H. Brune, W., Eisele, F., Tanner, D., Jefferson, A., … Williams, E. (1997). HO2/OH and RO2/HO2 ratios during the Tropospheric OH Photochemistry Experiment: Measurement and theory. Journal of Geophysical Research (Vol. 102). https://doi.org/10.1029/96JD01704

Walega, J. G., Dye, J. E., Grahek, F. E., & Ridley, B. K. (1991). Compact measurement system for the simultaneous determination of NO, NO2, NOy, and O3 using a small aircraft. In *Proc.SPIE* (Vol. 1433). Retrieved from https://doi.org/10.1117/12.46167

Washenfelder, R. A., Wagner, N. L., Dube, W. P., & Brown, S. S. (2011). Measurement of Atmospheric Ozone by Cavity Ring-down Spectroscopy. *Environmental Science & Technology*, *45*(7), 2938–2944. https://doi.org/10.1021/es103340u

Weinheimer, A. J., Walega, J. G., Ridley, B. A., Sachse, G. W., Anderson, B. E., & Collins Jr., J. E. (1993). Stratospheric NOy measurements on the NASA DC-8 during AASE II. *Geophysical Research Letters*, *20*(22), 2563–2566. https://doi.org/10.1029/93GL02627

Wild, R. J., Edwards, P. M., Dubé, W. P., Baumann, K., Edgerton, E. S., Quinn, P. K., … Brown, S. S. (2014). A Measurement of Total Reactive Nitrogen, NOy, together with NO2, NO, and O3 via Cavity Ring-down Spectroscopy. *Environmental Science & Technology*, *48*(16), 9609–9615. https://doi.org/10.1021/es501896w

Wooldridge, P. J., Perring, A. E., Bertram, T. H., Flocke, F. M., Roberts, J. M., Singh, H. B., … Cohen, R. C. (2010). Total Peroxy Nitrates (;PNs) in the atmosphere: the Thermal Dissociation-Laser Induced Fluorescence (TD-LIF) technique and comparisons to speciated PAN measurements. *Atmos. Meas. Tech.*, *3*(3), 593–607. https://doi.org/10.5194/amt-3-593-2010

Zhou, X., Gao, H., He, Y., Huang, G., Bertman, S. B., Civerolo, K., & Schwab, J. (2003). Nitric acid photolysis on surfaces in low-NOx environments: Significant atmospheric implications. *Geophysical Research Letters*, *30*(23). https://doi.org/10.1029/2003GL018620

Zhu, C., Xiang, B., Chu, L. T., & Zhu, L. (2010). 308 nm Photolysis of Nitric Acid in the Gas Phase, on Aluminum Surfaces, and on Ice Films. *The Journal of Physical Chemistry A*, *114*(7), 2561–2568. https://doi.org/10.1021/jp909867a